Supporting Information

Channelization of cathode/electrolyte interphase to enhance the rate-capability of $LiCoO_2$

Liewu Li,‡[ab] Zhencheng Huang,‡[a] Qi Yuan,[a] Hongbin Wang,[a] Xuming Yang,[a] Chufang Chen,[a] Xiaoyu Gong,[a] Qianqian Jiang,[a] Jing Chen,[c] Xiaoping Ouyang,[c] Jionghui Wang,[d] Liqing He,[e] Xiangzhong Ren,[a] Jiangtao Hu,[a] Qianling Zhang*[a] and Jianhong Liu*[ab]*

Experimental section

Material preparation

The $LiCoO_2$ was prepared using a previously reported method[1]. $ZrO(NO_3)_2{\cdot}H_2O$ and $NH_4H_2PO_4$ was obtained from Shanghai Aladdin Biochemical Technology Co., Ltd, and used without any additional purification steps.

As shown in **Fig. S1**†, the synthesis of the $LiCoO_2@ZrP_2O_7$ composite involved the following steps: Firstly, 1 g of $LiCoO_2$ was dispersed in 100 mL of deionized water through ultrasonication; secondly, specific amounts of $ZrO(NO_3)_2{\cdot}H_2O$ and $NH_4H_2PO_4$ (based on n (Zr) = 2 × n (P)) were added to the cloudy suspension of $LiCoO_2$ (with a ZrP_2O_7 content of 1.0 wt%), followed by stirring at 105 ℃ until complete solvent evaporation, resulting in the formation of a precursor powder with Zr^{4+}/PO_4^{3-}-coating on $LiCoO_2$. Thirdly, the obtained precursor powder with Zr^{4+}/PO_4^{3-}-coating on $LiCoO_2$ was calcined in air at 950 ℃ for 5 h, and then cooled to room temperature. Finally, grinding was performed to obtain the desired $LiCoO_2@ZrP_2O_7$ composite material. The same procedure was employed for the preparation of ZrP_2O_7 samples, as well as $LiCoO_2@ZrP_2O_7$-0.5 wt% (with a ZrP_2O_7 content of 0.5 wt%) and $LiCoO_2@ZrP_2O_7$-1.5 wt% (with a ZrP_2O_7 content of 1.5 wt%).

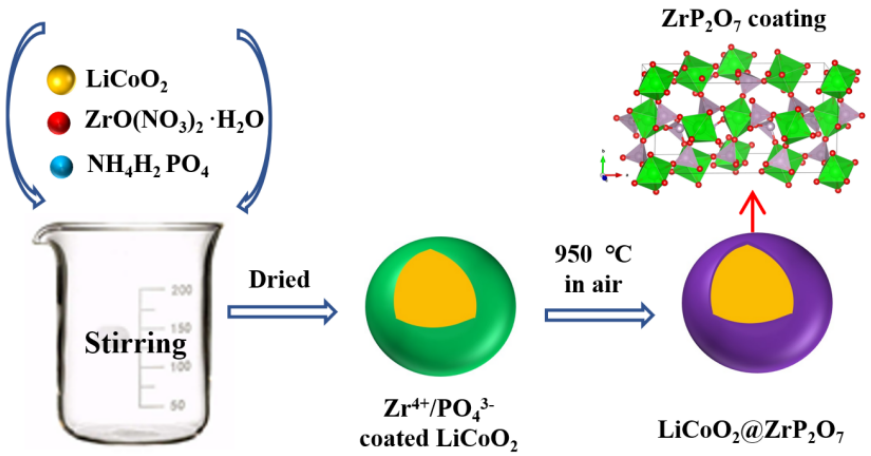

Fig. S1 Schematic representation of the synthesis process for the $LiCoO_2@ZrP_2O_7$.

Material characterization

The samples were subjected to X-ray diffraction (XRD) analysis using Cu-Kα radiation as the source. The refined XRD data were obtained through the application of the Rietveld method. Field-emission scanning electron microscopy (SEM) was employed for morphological characterization, while transmission electron microscopy (TEM) was utilized to examine the microstructures of the prepared materials. The quantity of ZrP_2O_7 present in the samples was determined using inductively coupled plasma optical emission spectrometry (ICP-OES) on an Agilent 730 instrument. Surface composition investigation was conducted via X-ray photoelectron spectroscopy (XPS).

Electrochemical measurements

The slurry, consisting of 80 wt% active material, 10 wt% PVDF, and 10 wt% acetylene black, was uniformly applied onto an aluminum foil current collector. The coated electrodes were then vacuum dried at a temperature of 120 ℃ overnight. The cathode had an approximate loading of active material at 1.0 mg cm^{-2}. For the assembly of CR2032 coin-type cells, a liquid electrolyte was used which comprised of a mixture of EC/DEC (1:1 v/v) with $LiPF_6$ dissolved in it at a concentration of 1 M along with 5 wt% FEC. To serve as the counter electrode, lithium foil was utilized while Celgard polymer membrane acted as the separator between the electrodes. Galvanostatic cycling tests were performed within the voltage range of 3.0-4.5 V vs Li^+/Li using a battery testing system (LAND CT2001A) maintained at a temperature of 25 ℃. Cyclic voltammetry (CV) measurements were conducted on an electrochemical workstation (CHI760E) under room temperature conditions within

the same voltage range as galvanostatic cycling tests. In situ electrochemical impedance spectroscopy (EIS) tests were conducted using a Solartron electrochemical workstation from the United States. The voltage range for charging and discharging was set between 3.0 V and 4.5 V, with a current density of 0.2C. Prior to the *in situ* EIS test, the cells underwent multiple cycles at a constant current density. Matlab software was utilized for performing distribution of relaxation time (DRT) transformations, ensuring consistent parameters throughout the calculations to maintain DRT result consistency.

Computation Methods

The VASP code, based on density functional theory (DFT)[2, 3], was utilized for conducting the simulations. The ion-electron interaction employed the projector-augmented wave (PAW) method, while the exchange-correlation interaction was determined using the generalized gradient approximation (GGA) PBE functional[4]. To simulate ZrP_2O_7 bulk, a plane wave cutoff energy of 400 eV and a Monkhorst-Pack (MP)[5] k-point mesh of 7 × 7 × 7 were implemented. All atomic positions underwent relaxation until achieving an energy change below 0.1 meV and force less than 0.01 eV/Å on each atom. Additionally, spin-polarization was considered in this calculation, and diffusion barriers were determined using the Climbing Image Nudged Elastic Band (CI-NEB) method[6].

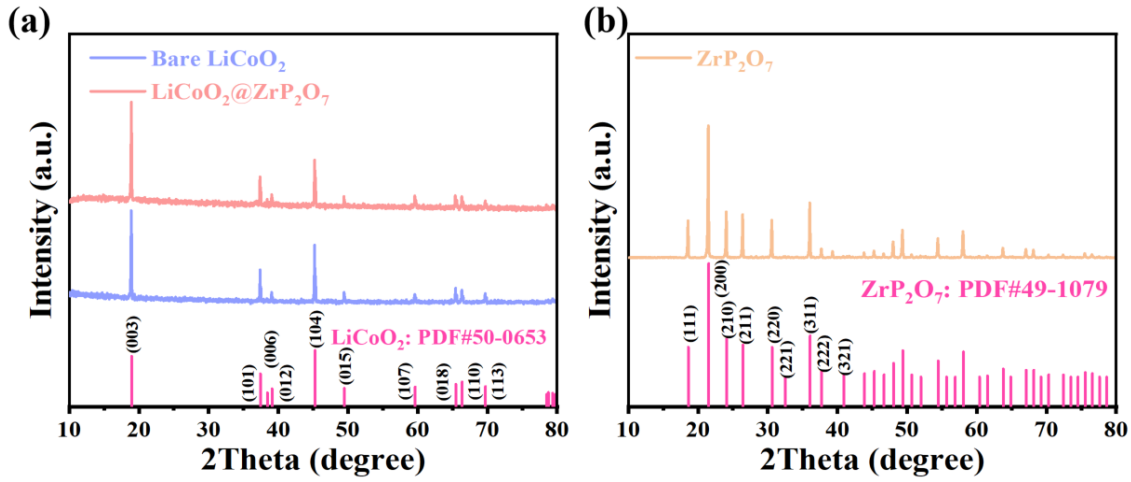

Fig. S2 (a) The XRD patterns of the bare $LiCoO_2$, $LiCoO_2$@ZrP_2O_7 and **(b)** ZrP_2O_7.

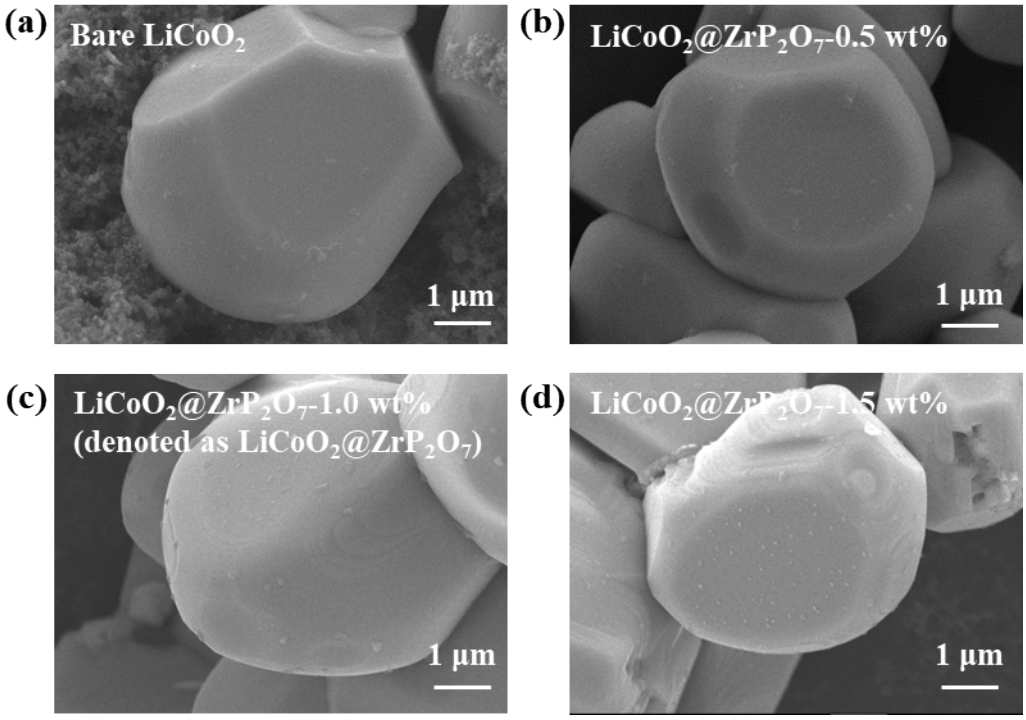

Fig. S3 SEM images of the **(a)** bare $LiCoO_2$, **(b)** $LiCoO_2@ZrP_2O_7$-0.5 wt%, **(c)** $LiCoO_2@ZrP_2O_7$-1.0 wt% (denoted as $LiCoO_2@ZrP_2O_7$), and **(d)** $LiCoO_2@ZrP_2O_7$-1.5 wt%.

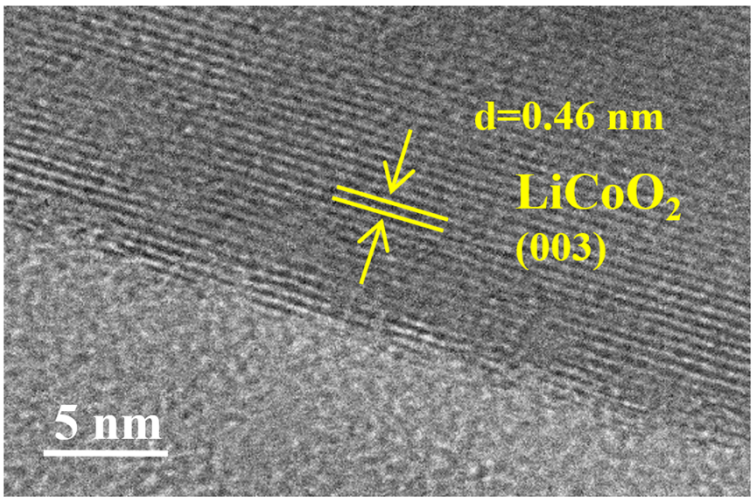

Fig. S4 High-resolution TEM image of the bare $LiCoO_2$.

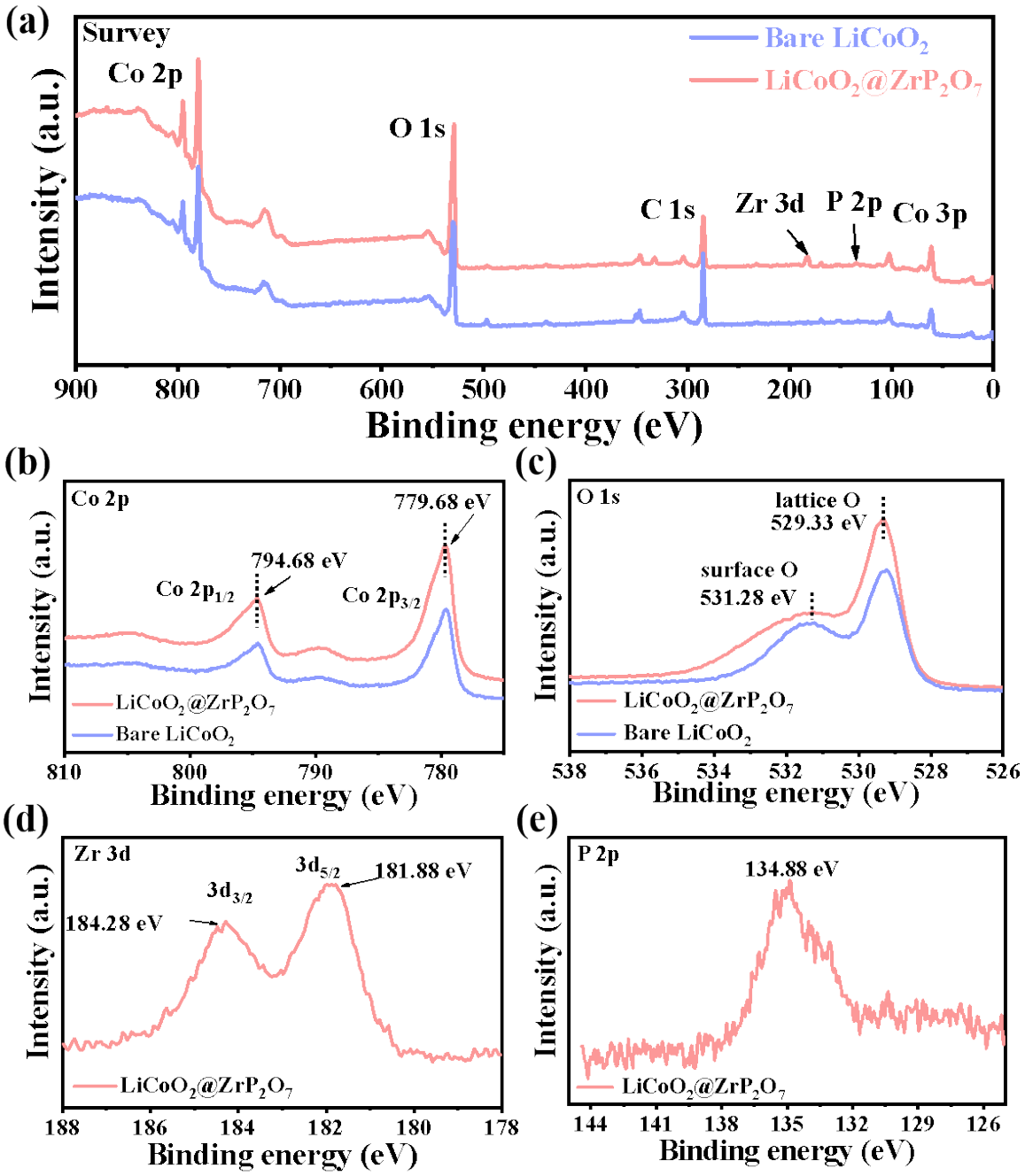

Fig. S5 (a) The XPS spectrum of the bare $LiCoO_2$ and $LiCoO_2@ZrP_2O_7$. High-resolution XPS spectra of **(b)** Co 2p and **(c)** O 1s for the bare $LiCoO_2$ and $LiCoO_2@ZrP_2O_7$. High-resolution XPS spectra of **(d)** Zr 3d and **(e)** P 2p for the $LiCoO_2@ZrP_2O_7$.

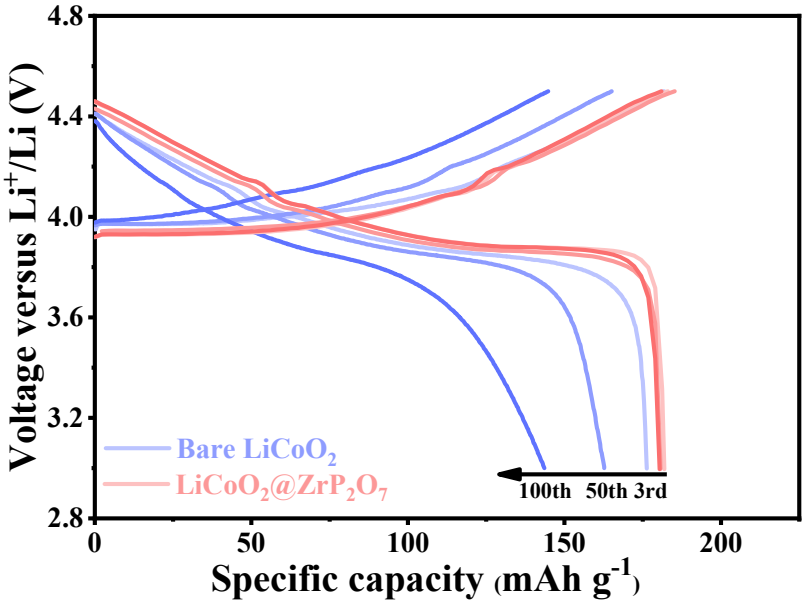

Fig. S6 Voltage profiles of the bare $LiCoO_2$ and the $LiCoO_2@ZrP_2O_7$ at 0.5C.

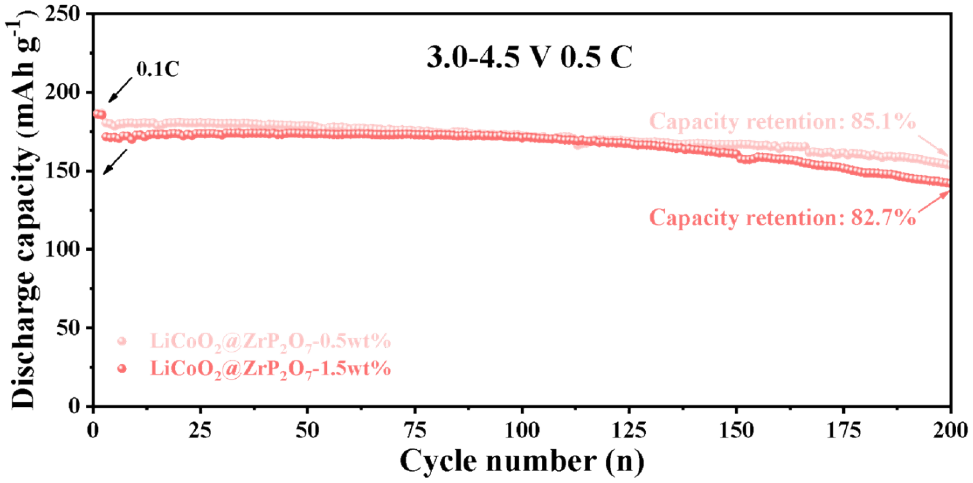

Fig. S7 Long-term cycling performance of the $LiCoO_2@ZrP_2O_7$-0.5 wt% and the $LiCoO_2@ZrP_2O_7$-1.5 wt% at 0.5C.

Table S1 The test data of ICP-OES analysis for $LiCoO_2@ZrP_2O_7$.

Sample name	Test element	Test element concentration C_0 (mg L^{-1})	Dilution ratio (f)	Element concentration of digestion solution/original sample solution C_1 (mg L^{-1})	Sample element content C_x (mg kg^{-1})	Sample element content W(%)
$LiCoO_2@ZrP_2O_7$	Co	4.34	1000	4339.11	599324.59	59.93%
	P	0.16	100	16.25	2244.17	0.22%
	Zr	0.16	100	15.71	2170.51	0.22%

Table S2 Refined structural parameters of the bare $LiCoO_2$ and $LiCoO_2@ZrP_2O_7$.

Samples	**a(Å)**	**c(Å)**	**z_{ox}[a]**	**V(Å^3)**	**$S_{(MO2)}$ (Å)[b]**	**$I_{(LiO2)}$ (Å)[c]**	**R_p (%)**	**R_{wp} (%)**
Bare $LiCoO_2$	2.8135(5)	14.0406(7)	0.2593(4)	96.25(7)	2.0789	2.6013	1.64	1.94
$LiCoO_2@ZrP_2O_7$	2.8161(1)	14.0051(6)	0.3001(6)	96.50(6)	1.9308	2.7376	0.95	1.41

a z_{ox} is the oxygen position at 6c sites.

b Slab thickness: $S(MO_2) = 2[(1/3) - z_{ox}]c$.

c Interslab space thickness: $I_{(LiO2)} = (c/3) - S_{(MO2)}$.

Table S3 Different resistances calculated by DRT analysis from the EIS in **Fig. 3g** and **h**.

	1st cycle of the $LiCoO_2$	**1st cycle of the $LiCoO_2@ZrP_2O_7$**	**10th cycle of the $LiCoO_2$**	**10th cycle of the $LiCoO_2@ZrP_2O_7$**
R_{EC} (Ω)	51.73	15.36	12.02	0.82
R_{CEI} (Ω)	46.19	30.32	23.35	10.21
R_{CT} (Ω)	64.08	66.49	56.64	38.77

References

1. L. Li, Q. Yuan, S. Ye, Y. Fu, X. Ren, Q. Zhang and J. Liu, In situ formed lithium ionic conductor thin film on the surface of high-crystal-layered $LiCoO_2$ as a high-voltage cathode material, *Mater. Chem. Front.,* 2021, **5**, 6171-6181.

2. G. Kresse and J. Hafner, Ab initio molecular dynamics for liquid metals, *Phys. Rev. B*, 1993, **47**, 558-561.

3. P. Hohenberg and W. Kohn, Inhomogeneous Electron Gas, *Phys. Rev.*, 1964, **136**, B864.

4. J. P. Perdew, J.A. Chevary, S.H. Vosko, K. A. Jackson, M.R. Pederson, D.J. Singh, C. Fiolhais, Atoms, molecules, solids, and surfaces: Applications of the generalized gradient approximation for exchange and correlation, *Phys. Rev. B*, 1992, **46**, 6671-6687.

5. H. Monkhorst and J. Pack, Special points for Brillouin-zone integrations, *Phys. Rev. B*, 1976, **13**, 5188-5192.

6. G. Henkelman, B. Uberuaga and H. Jónsson, A climbing image nudged elastic band method for finding saddle points and minimum energy paths, *J. Chem. Phys.*, 2000, **113**, 9901-9904.